SAN099-0662C

~~DRAFT 8/19/99~~

Z-Pinch Generated X-Rays in Static-Wall-Hohlraum Geometry Demonstrate Potential for Indirect-Drive ICF Studies*

T. W. L. Sanford, R. E. Olson, G. A. Chandler, D. E. Hebron, R. C. Mock, R. J. Leeper, T. J. Nash, L. E. Ruggles, W. W. Simpson, K. W. Struve, and R. A. Vesey
Sandia National Laboratories, P. O. Box 5800, Albuquerque, New Mexico 87185

R. L. Bowers, W. Matuska, and D. L. Peterson
Los Alamos National Laboratory, Los Alamos, New Mexico 87545-0010

R. R. Peterson
Univerisity of Wisconsin

Abstract

Hohlraums of full ignition scale (6-mm diameter by 7-mm length) have been heated by x-rays from a z-pinch target on Z to a variety of temperatures and pulse shapes which can be used to simulate the early phases of the National Ignition Facility (NIF) temperature drive. The pulse shape is varied by changing the on-axis target of the z pinch in a static-wall-hohlraum geometry [*Fusion Technol.* 35, 260 (1999)]. A 2-μm-thick walled Cu cylindrical target of 8-mm diameter filled with 10 mg/cm^3 CH, for example, produces *foot-pulse* conditions of ~85 eV for a duration of ~10 ns, while a solid cylindrical target of 5-mm diameter and 14-mg/cm^3 CH generates *first-step-pulse* conditions of ~122 eV for a duration of a few ns. Alternatively, reducing the hohlraum size (to 4-mm diameter by 4-mm length) with the latter target has increased the peak temperature to ~150 eV, which is characteristic of a *second-step-pulse* temperature. In general, the temperature T of these x-ray driven hohlraums is in agreement with the Planckian relation $T \sim (P/A)^{1/4}$. P is the measured x-ray input power and A is the surface area of the hohlraum. Fully-integrated 2-D radiation-hydrodynamic simulations of the z pinch and subsequent hohlraum heating show plasma densities within the useful volume of the hohlraums to be on the order of air or less.

DISCLAIMER

1. INTRODUCTION

Radiation environments characteristic of those encountered during the low-temperature *foot pulse* and subsequent higher-temperature *early-step pulses* (Fig. 1) required for indirect-drive ICF ignition on NIF [1, 2] are desired in order to provide a platform to better understand the dynamics of NIF hohlraums and capsules prior to NIF completion [3]. In particular, (1) the dynamics of the proposed He-fill wall tamping and hole closure in the NIF hohlraum, and (2) improved capsule ablator burn-through rates and shock propagation velocities [4] are needed to better design these components. In this paper, we show that an axial hohlraum using the static-wall-hohlraum geometry [5] heated by x-rays from a z-pinch on the Z generator [6] is capable of providing environments for such pre-NIF studies.

In this single-sided x-ray drive (Fig. 2), the axial hohlraum is placed above a central hohlraum in an x-ray-producing z-pinch. X-rays produced in the central hohlraum enter the axial hohlraum through a radiation-entrance-hole (REH) and heat its walls. The x-rays are generated in the central hohlraum by the thermalization of the kinetic energy acquired when a cylindrical plasma shell, created by one or more wire arrays, collides with a pulse-shaping target (PST) within the z-pinch. In this arrangement, the wires (which are made of W) form an annular plasma radiation case [7] by the time they strike the PST (first strike). The high-atomic-number radiation case traps a fraction of the x-rays produced in a central hohlraum formed from the PST (as in a dynamic-hohlraum [8]), and radiation flows from the interior of the PST into the axial hohlraum, whose walls remain relatively static. A foam fill is used in the PST so that as final stagnation is approached, the foam will remain transparent to the x-rays, yet provide a back-pressure on the imploding mass. The back-pressure enables additional energy to be extracted from the acceleration and increases the x-ray energy generated as the magnetic field compresses the PST.

2. EXPERIMENTAL ARRANGEMENT

Figure 2 illustrates the geometry used for the single-sided x-ray drive discussed here, and points out the location of the wire-array z-pinch load at the terminus of the Z generator, the PST (which forms the central hohlraum), the REH, and the axial hohlraum. The use of large numbers of wires in arrays is essential for generating high radiated powers from z-pinches [9]. Nesting the arrays, moreover, enhances the power in targetless pinches [10]. Accordingly, the load in these experiments is made of outer and inner arrays of wire that number 240 and 120, respectively. In Z the load current ramps to a peak of ~20 MA in ~100 ns. The associated array diameters of 40 mm and 20 mm, array masses of 2 mg and 1 mg, and wire length of ~10 mm are designed to approximately optimize the coupling of the generator's magnetic energy into kinetic energy of the arrays prior to stagnation. The path of the current return is through the outside of the cylindrical anode (A in Fig. 2A)), which is solid except for a 3-mm diameter diagnostic aperture having conducting wires spaced every mm (Fig. 2C). This design minimizes the azimuthal magnetic perturbation on the imploding array, but still permits the monitoring of the radiation generated outside the implosion. To minimize W plasma sliding across the REH and blocking the radiation generated in the central hohlraum from entering the axial hohlraum [11], the anode is slanted 3 degrees to the horizontal between the inner array and the PST (Fig. 2B). To maintain symmetry, the cathode is similarly slanted (Fig. 2A).

The axial hohlraums used are thin-walled (25.4-μm thickness) Au cylinders, measuring either 6-mm in diameter by 7-mm in height (ignition scale [Fig. 2A]) or 4-mm in both diameter and height. The axial hohlraum temperature is measured with two independent diagnostics, each of which views the interior wall of the hohlraum through the same aperture (~3-mm diameter for the large hohlraum or 2-mm diameter for the small hohlraum), but at $\pm 20^{0}$ about the normal to the hole in the horizontal plane. In one diagnostic, the temperature is measured using a set of twelve silicon-diodes mounted downstream from a transmission-grating-spectrometer, which is positioned to be sensitive to x-rays in discrete energy channels spanning 100 to 600 eV. In the other diagnostic, the

temperature is measured using a total-energy bolometer and a set of K- and L-edge filtered x-ray diodes (XRDs) sensitive to x-rays in four discrete channels covering a similar energy range [6]. Plasma closure of the diagnostic hole with time is measured with a multi-filtered, fast-framing, pin-hole camera (PHC) sensitive to x-rays in four discrete spectral channels covering 100 to 600 eV [12]. Relative comparisons between the radiation detectors within each diagnostic set indicate no measurable deviation in internal azimuthal symmetry of the hohlraum with time. The peak temperature extracted from either diagnostic set agrees to within 2%±3% when averaged over the shots taken. The uncertainty refers to the RMS shot-to-shot variation. For the temperatures discussed here, a correction for the reduced hole size with time based on the averages of these images is used. The radiation entering the hohlraum is estimated by an additional suite of on-axis diagnostics [8] that view the source through the REH when the hohlraum is not present (Fig. 2A). These diagnostics include a total-energy bolometer, a filtered XRD set, and filtered fast-framing PHCs similar to those detectors of the horizontal diagnostic sets. Over the measured x-ray input powers P of 0.7 to 13 TW, the hohlraum temperature T scales as the Planckian relation $T \sim (P/A)^{1/4}$, where A is the surface area of the hohlraum (Fig. 3). In Fig. 3, all the data except the highest temperature datum of ~150 eV correspond to those measured with the 6x7-mm^2 hohlraum.

The PSTs are are constructed with a thin metal (Cu or Au) outside shell surrounding a CH-foam cylinder. The range of shell thickness, foam density, and diameter fielded includes 0-18 μg/cm^2, 0-14 mg/cm^3, and 0-8 mm, respectively. In general, increasing the diameter of the PST or mass of its components increases the duration and risetime of the x-ray pulse delivered to the hohlraum prior to final stagnation, and simultaneously decreases the initial on-axis x-ray power. For a PST of 8-mm diameter filled with 6 mg/ cm^3 foam, for example, increasing the thickness of the shell from 0 to 18 μg/cm^2 increases the pulse duration from 8 to 18 ns, the risetime from 3 to 7 ns, and reduces the peak x-ray power from 7 to 1 TW (Fig. 4). Radiation exterior to the PST is monitored through a small aperture (Fig. 2C) in the current return can with a suit of off-axis diagnostics similar to that of the on-axis suite (Fig. 2A).

3. HOHLRAUM TEMPERATURE PULSE SHAPES

Figure 1 illustrates two representative temperature pulse shapes designed to ignite 2-mm diameter Be-coated capsules on NIF. In the figure, W and D correspond to the 300-eV peak-temperature and reduced peak-temperature drive of Refs. 13 and 14, respectively. Shown also in the figure are three temperature pulse shapes measured with two different PSTs and the two different hohlraum sizes. Shots Z252 and Z441 use the 6x7-mm^2 hohlraum, while Z442 uses the 4x4-mm^2 hohlraum. Shot Z252 uses a 5.8-mm diameter REH with a PST of 8 mm diameter and a 18-μg/cm^2 Cu shell filled with 10 mg/cm^3 foam. Shots Z441 and Z442 use a 4-mm diameter REH with a 5-mm diameter PST constructed solely of 14-mg/cm^3 foam. The temperature field generated with the larger-diameter, more-massive PST matches the field required for simulating the ~85 eV, ~10-ns *foot pulse* in the NIF-scale hohlraum. The field generated with the less massive target, in contrast, provides a reasonable match for simulating the temperature associated with the *first-step pulse*. Because the solid foam target permits the pinch to compress to ~0.5-mm radial dimensions, smaller hohlraums with reduced diameters can also be efficiently heated with this target and therefore driven to yet higher temperatures. Thus, alternatively, reducing the hohlraum size with this target enables the higher temperature associated with the *next step* to be reached, as shown by the measured temperature history Z442 in Fig. 1.

4. HOHLRAUM CHARACTERISTICS

Radiation-magnetohydrodynamic code (RMHC) simulations such as those of Ref. 11 are used to understand the underlying dynamics of the implosion, and to provide insight into the radiation and plasma fields inside the axial hohlraum. These simulations are 2-D integrated calculations that take into account the development of the Rayleigh-Taylor instability in the r-z plane of the imploding load, energy generation as the plasma assembles on the PST, and radiation transport (in the diffusion approximation) to the axial hohlraum. Figure 5 plots the simulated radiation and lower bound on the wall temperature (at an optical depth of 0.66) of the axial hohlraum 4 mm above the

REH, for example, corresponding to the conditions of shot Z441. According to the simulation, the hohlraum is first bathed in a low-temperature field of ~30-40 eV (radiation pre-pulse), once the outer array strikes the inner array at ~214 ns. When the leading edge of the combined imploding plasma shell next strikes the outer edge of the PST at ~227 ns, the power entering the hohlraum rises rapidly and the associated temperature of the hohlraum quickly increases to >120 eV by ~231.5 ns. At this time, the plasma bubbles associated with the W shell have just begun to stagnate on axis. The continued rise in the temperature between ~231.5 and 234 ns corresponds to the 2-D stagnation of the bubbles on axis during this final stagnation process. Maximum simulated and measured total-radiated off-axis power have been synchronized so that the peaks occur at 234 ns. The measured temperature profiles shown in Fig. 1 all arise during the heating between the first strike on the foam and the beginning of the bubbles stagnating on axis. Experimentally, the magnitude of the calculated temperature enhancement during final stagnation is not observed for any of the PSTs, as illustrated in the comparison shown in Fig. 5. The absence of the enhancement in the measurements relative to the simulation may be due to: (1) 3-D effects not included in the 2-D simulation; (2) underestimates of the opacity within the compressing PST; (3) inadequacy of the diffusion approximation during pinch; (4) reduced radiation containment by the tungsten plasma during pinch; (5) underestimates of ablative closure of the REH; (6) additional tungsten sliding across the REH [11]; or possibly (7) the inadequacy of the model to predict the details of the pinch. Enabling the enhancement to occur would permit multiple-step pulses to be simulated as well as just the single steps shown in Fig. 1. The simulations suggest, however, that even with the calculated enhancement the plasma filling the hohlraum is minimal. For the Z441 simulation of Fig. 5., for example, between 231.5 and 234 ns the calculated radius of the REH has been reduced by only 0.04 to 0.2 mm, the Au wall (4 mm above the REH) has expanded radially by only 0.04 to 0.25 mm into the interior of the hohlraum, and the W plasma has expanded axially through only the ~0.5-mm depth of the REH aperture, with only CH plasma entering the axial hohlraum. Figure 6 plots the density of this CH plasma in the axial hohlraum 2 mm above the REH, and shows that the density remains low, about that of air, for the duration of the temperature rise.

5. CONCLUSIONS

In conclusion, the measurements made with this single-sided-drive, static-wall-hohlraum geometry on Z have shown the ability to generate temperature pulse shapes of utility to pre-NIF studies up to peak temperatures of ~130 eV in full ignition-scale hohlraums, and ~150 eV in reduced scale hohlraums. The RMHC simulations, like those of the measurements [16] suggest that over useful radiation drive times, the main volume of the hohlraums remains relatively free of z-pinch plasma. Although the 2-D simulations are useful, a number of discrepancies remain between the behavior calculated and measured.

If, instead of a single pinch, the wire mass were to be distributed in two independent pinches of roughly half the length of a single one (in order to maintain a similar over-all load inductance) with the axial hohlraum sandwiched between the two, the power entering the hohlraum would be roughly doubled because the on-axis power is generated primarily near the pinch ends. The peak temperature associated with this single-feed, but now two-sided x-ray drive (as in the geometry shown in Fig. 3 of Ref.5) would then be increased to 155 eV for the 6x7-mm^2 hohlraum [15] or ~180 eV for the 4x4-mm^2 hohlraum. Scaling this concept to a 50-MA driver, which is characteristic of the next generation z-pinch driver being considered [17], moreover, could thus provide conditions for studying implosions driven at peak temperatures in the range of 240-280 eV, depending on hohlraum size.

References:

[1] S. W. Hann, et al , *Phys. Plasmas* 2, 2480 (1995).

[2] W. J. Krauser, et al , *Phys. Plasmas* 3, 2084 (1996).

[3] J. D. Kilkenny, T. P. Bernat, B. A. Hammel, et al, *Laser and Particle Beams* 17,159-171 (1999).

[4] R. E. Olson, *et al.*, *Phys. Plasmas* 4, 1818 (1997).

[5] R. E. Olson, et al., *Fusion Technology* 35, 260 (1999).

[6] R. B. Spielman, et al., *Phys. Plasmas* 5, 2105 (1998).

[7] T. W. L. Sanford, *et al.*, *IEEE Trans. Plasma Sci.* 26, 1086 (1998).

[8] T. J. Nash , et al, *Phys. Plasmas* 6, 2023 (1999).

[9] T. W. L. Sanford , et al, *Phys. Plasmas* 6, xxxx (May 1999).

[10] C. Deeney, et al, *Phys. Rev. Lett.* 81, 4883 (1998).

[11] D. L. Peterson, et al, *Phys. Plasmas* 6, 2178 (1999).

[12] L. E. Ruggles, et al, *Rev. Sci. Instrum.* 66, 712,(1995).

[13] D. C. Wilson, et al, *Phys. Plasmas* 5, 1953 (1998).

[14] T. R. Dittrich, et al, *Phys. Plasmas* 5, 3708 (1998).

[15] T. W. L. Sanford, R. E. Olson, G. A. Chandler, et al, "Z-Pinch Generated X-Rays Demonstrate Potential of Indirect Drive ICF Experiments", submitted to *Phys. Rev. Letts.* (July 1999).

[16] R. J. Leeper, T. E. Alberts, J. R. Asay, et al, "Z-Pinch Driven Inertial Confinement Fusion Target Physics Resarch at Sandia National Laboratories", to be published *Nuclear Fusion* (1999).

[17] K. W. Struve, et al,"ZX Pulsed-Power Design," to be published in the *Proceedings of the International Pulsed Power Conference, 1999, Monterey, CA* (June 1999).

*Sandia is a multiprogram laboratory operated by the Sandia Corporation, a Lockheed Martin Company, for the U.S. Department of Energy under Contract No. DE-AC04-94AL85000.

Figure Captions:

1. Comparison of representative NIF radiation temperature profiles (W and D) with those measured for Shots Z251, Z441, and Z442.

2. Schematic of single-sided, static-wall-hohlraum geometry .

3. Measured hohlraum temperature as a function of the measured on-axis x-ray power without the hohlraum present, for the indicated shot pairs. Shown also is that expected from the $T\sim(P/A)^{1/4}$ Planckian relation, using a calculated normalization point at 13-TW [15].

4. Peak power, risetime, and duration to final stagnation of measured on-axis x-ray pulse versus shell thickness, for a 8-mm diameter PST with 6 mg/cc foam fill.

5. Comparison of the simulated radiation and lower bound on the wall temperature with that measured for Shot Z441.

6. Simulated on-axis plasma density 2-mm above the REH for Shot Z441.

Static-Wall Hohlraum Can Simulate NIF Relevant Foot, First-Step, and Second-Step Radiation Drives

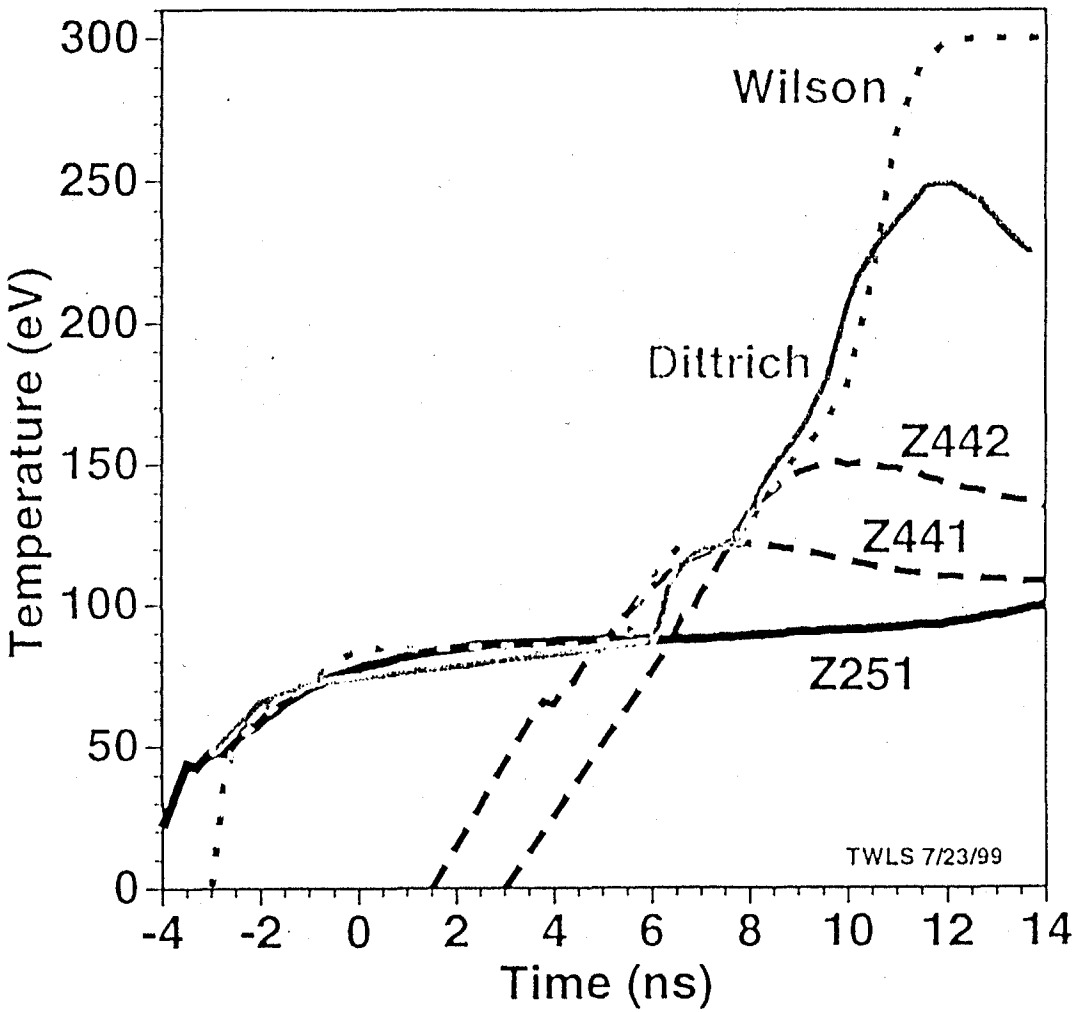

Fig. 1

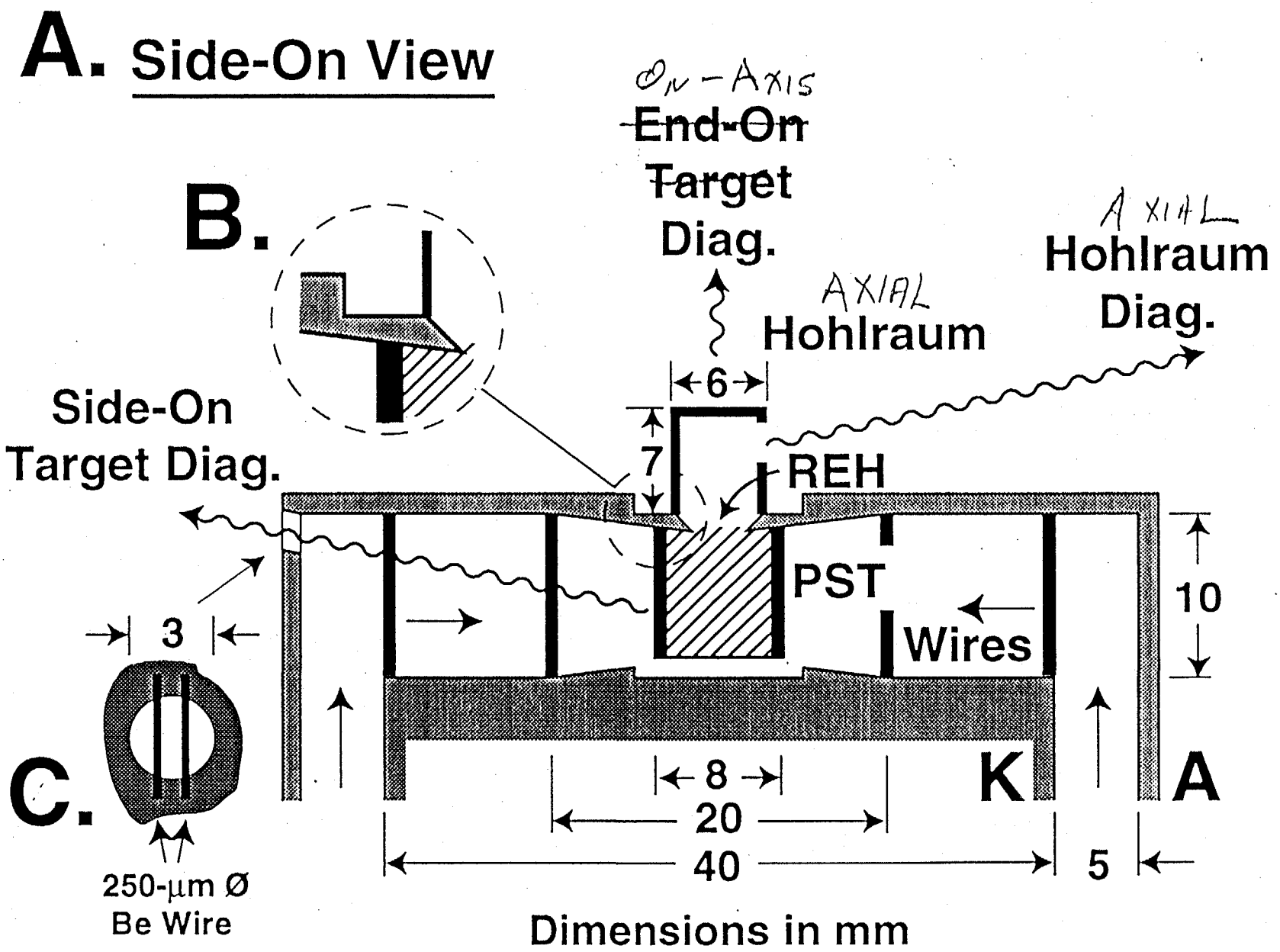
A. Side-On View
On-Axis
End-On
Target
Diag.
B.
AXIAL
Hohlraum
AXIAL
Hohlraum
Diag.
6
Side-On
Target Diag.
7
REH
PST
Wires
10
3
C.
8
K
A
20
40
5
250-μm Ø
Be Wire
Dimensions in mm

Fig. 2

Measured Temperature of NIF Sized (153 mm^2) Hohlraum vs Measured Incident On-Axis Power Agrees with Theory

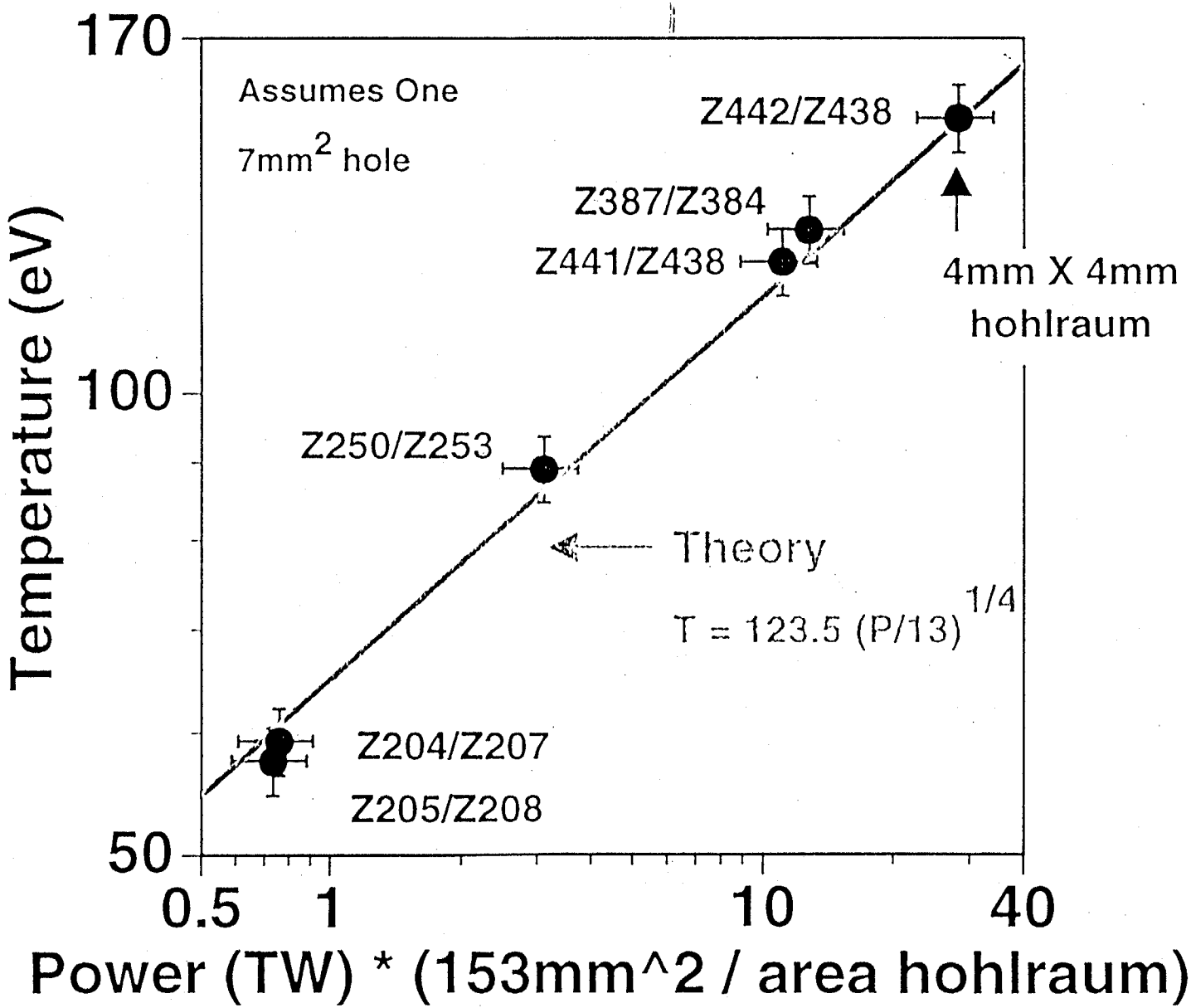

TWLS
7/20/99

Fig. 3

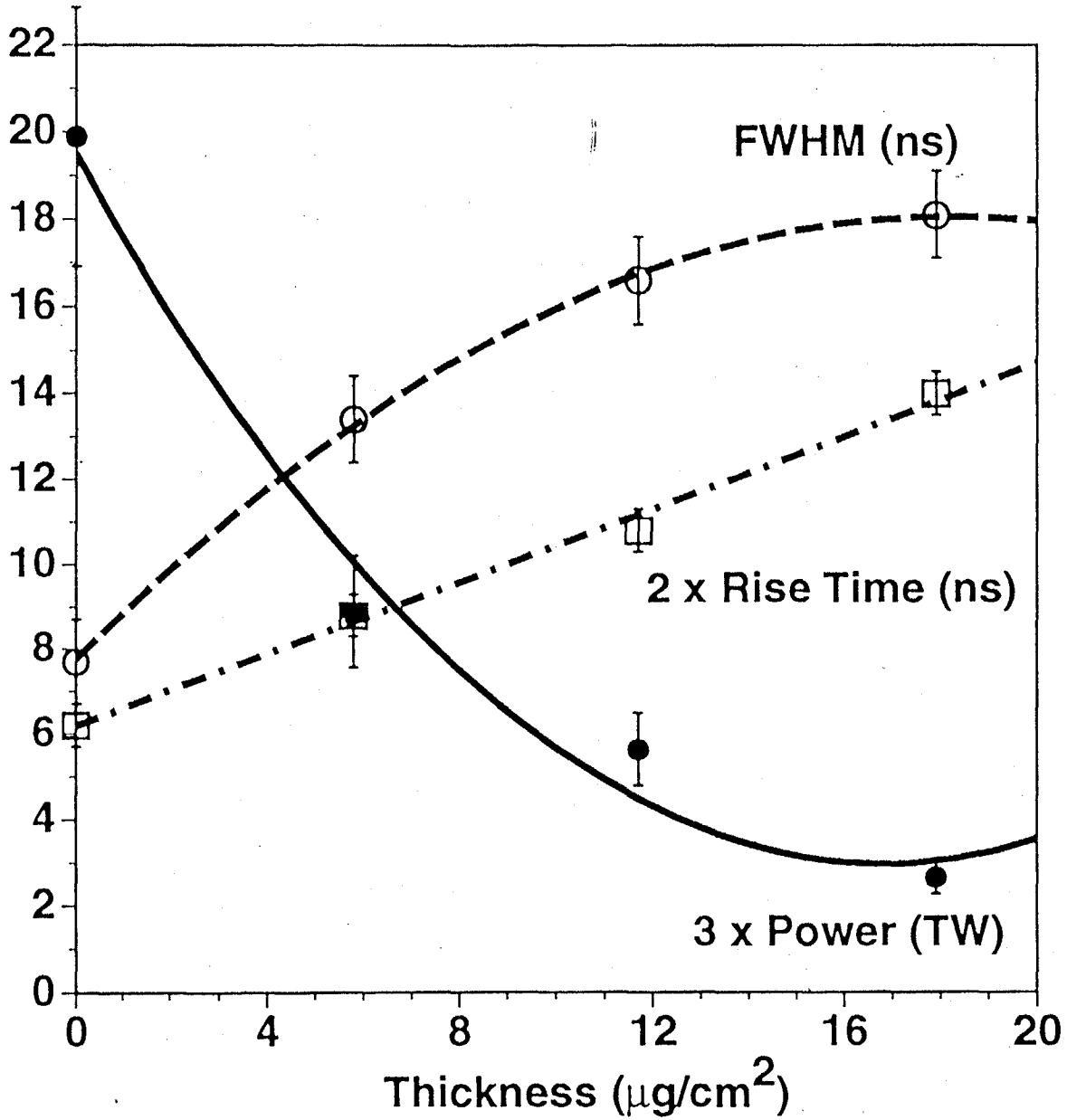
22
20
18
16
14
12
10
8
6
4
2
0
0
4
8
12
16
20
FWHM (ns)
2 x Rise Time (ns)
3 x Power (TW)
Thickness (μg/cm²)

Fig. 4

Measured (Simulated) Peak Temperature Occurs 0.3±1 ns (0 ns) Prior to Stagnation

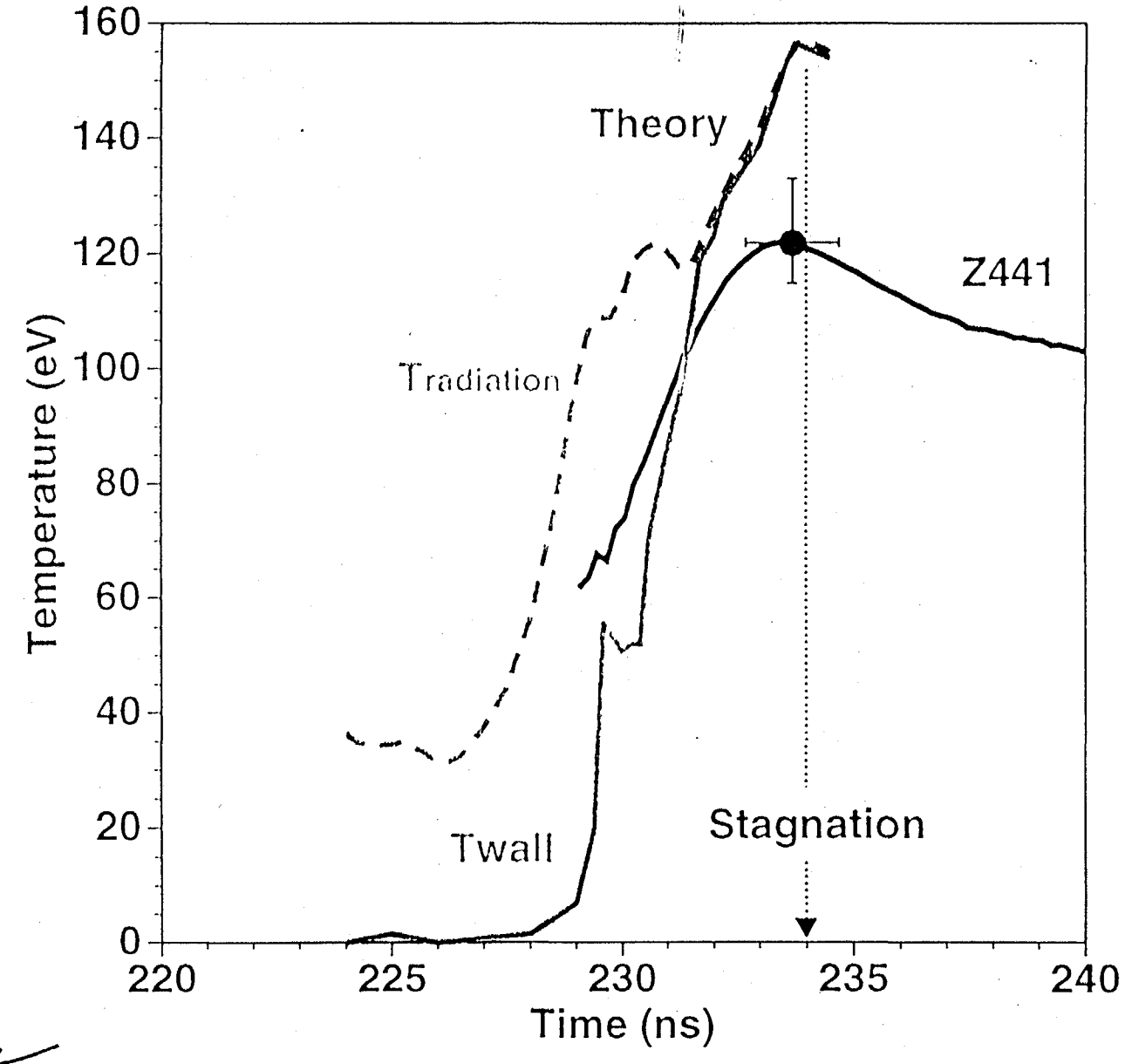

Fig. 5

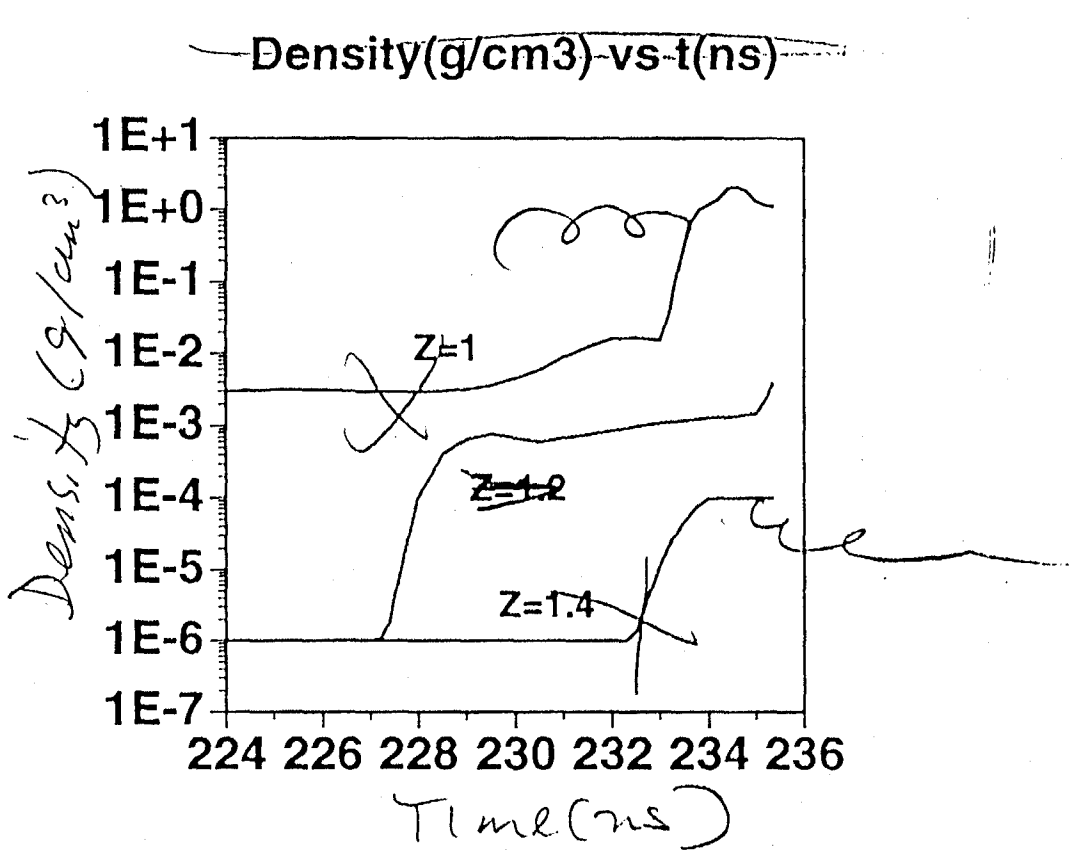
Density(g/cm3)-vs-t(ns)
1E+1
1E+0
1E-1
1E-2
1E-3
1E-4
1E-5
1E-6
1E-7
Z=1
Z=1.2
Z=1.4
224 226 228 230 232 234 236
Time(ns)

Fig 6